Transport of regional pollutants through a remote trans-Himalayan valley in Nepal

Shradda Dhungel[1], Bhogendra Kathayat[2], Khadak Mahata[3], Arnico Panday[1,4]

[1] Department of Environmental Sciences, University of Virginia, Charlottesville, VA 22904, USA
[2] Nepal Wireless, Shanti Marg, Pokhara, 33700, Nepal
[3] Institute for Advanced Sustainability Studies, Potsdam, 14467, Germany
[4] International Center for Integrated Mountain Development, Khulmaltar, Kathmandu, 44700, Nepal

Correspondence to: Shradda Dhungel (shradda@virginia.edu)

Abstract. Anthropogenic emissions from the combustion of fossil fuels and biomass in Asia have increased in recent years. High concentrations of reactive trace gases and light-absorbing and -scattering particles from these sources over the Indo-Gangetic Plain (IGP) of southern Asia form persistent haze layers, also known as atmospheric brown clouds, from December through early June. Models and satellite imagery suggest that strong wind systems within deep Himalayan valleys are major pathways by which pollutants from the IGP are transported to the higher Himalaya yet observational evidence of transport through Himalayan valleys has been lacking to date. To evaluate this pathway, we measured black carbon (BC), ozone (O_3), and associated meteorological conditions within the Kali-Gandaki Valley (KGV), Nepal, from January 2013 to July 2015. BC and O_3 varied over both diurnal and seasonal cycles. Relative to nighttime, mean BC and O_3 concentrations within the valley were higher during daytime when the up-valley flow (average velocity of 17 m s^{-1}) dominated. BC and O_3 concentrations also varied seasonally with minima during the monsoon season (July to September). Concentrations of both species subsequently increased post monsoon and peaked during March to May. Average concentrations for O_3 during April, August, and November were 41.7 ppbv, 24.5 ppbv, and 29.4 ppbv, respectively, while the corresponding BC concentrations were 1.17 µg m^{-3}, 0.24 µg m^{-3}, and 1.01 µg m^{-3}, respectively. Up-valley fluxes of BC were significantly greater than down-valley fluxes during all seasons. In addition, frequent episodes of BC concentrations two to three times higher than average persisted from several days to a week during non-monsoon months. Our observations of increases in BC concentration and fluxes in the valley, particularly during pre- monsoon, support the hypothesis that trans-Himalayan valleys are important conduits for transport of pollutants from the IGP to the higher Himalaya.

Keywords: black carbon, ozone, trans-Himalayan valleys, pollutant pathways, long-range transport, regional transport episodes, short-lived climate forcers.

1. Introduction

Persistent atmospheric haze, often referred to as Atmospheric Brown Cloud (ABC) (Ramanathan and Crutzen, 2003), affects broad geographic regions including the Indo-Gangetic plain (IGP) in southern Asia (Ramanathan and Carmichael, 2008), eastern China (Ma et al., 2010), southeast Asia (Engling and Gelencser, 2010), sub-Saharan Africa (Piketh et al., 1999), Mexico (Vasilyev et al., 1995), and Brazil (Kaufman et al., 1998). In southern Asia, the haze covers extensive areas particularly during the period of mid-November to mid-June preceding the summer monsoon season. Major combustion sources (primarily anthropogenic) including the burning of agricultural waste, garbage, biofuel, and fossil fuels as well as wildfires emit volatile and particulate-phase compounds to the atmosphere that contain oxidized and reduced forms of sulfur, nitrogen, and organic carbon (OC) together with elemental (black) carbon (BC) and other species. These emissions are intermixed and chemically interact with mechanically produced aerosols (e.g., sea salt and mineral dust). Important secondary pollutants such as ozone (O_3) form from photochemical reactions involving nitrogen oxides and volatile organic species are also produced. Together, this mixture of atmospheric species constitutes ABC or the brown haze in South Asia (Ramanathan et al., 2005; Gustafsson et al., 2009). These optically thick layers include high concentrations of light absorbing and light scattering particles (Menon et al., 2002) that modulate radiative transfer. Light absorbing aerosols (primarily BC and crustal dust) contribute to warming of the atmosphere while light scattering aerosols (primarily S-, N-, and OC dominated particles) drive cooling at the surface. The combined effects of light absorbing and light scattering aerosols from anthropogenic sources reduce UV and visible wavelength radiation at the surface (i.e., surface forcing), increase the warming of the troposphere (i.e., atmospheric forcing) and change the net top of the atmosphere solar flux (i.e., top-of-the-atmosphere forcing) (Andreae and Crutzen, 1997; Kaufman et al., 2002, Ramanathan et al., 2005). Light-absorbing anthropogenic pollutants like BC significantly influence global warming, in terms of direct radiative forcing (Jacobson, 2001; Bond et al., 2013); regional influences from such pollutants close to sources are greater than those on the global scale (Ramanathan et al., 2007b).

The elevated concentration of aerosols in the anti-cyclone also weakens the circulation pattern and reduces total monsoon precipitation over southern India (Ramanathan et al, 2005; Fadnavis et al., 2013) while intensifying the monsoon over the foothills of the Himalaya (Lau et al., 2006). In addition to warming the atmosphere, the rising concentrations of BC and O_3 over southern Asia (e.g., Ramanathan and Carmichael, 2008) have detrimental impacts on human health. The effects of BC on cardiopulmonary and respiratory problems are greater than those of PM 2.5 or 10 particles (Janssen et al., 2011). O_3 also compromises pulmonary function (Krupnick et. al, 1990) and is a leading pollutant causing biodiversity loss (Royal Society, 2008) and declining crop yields by directly damaging leaves (Auffhammer et al., 2006).

Most haze over the IGP often reaches heights of more than 3 km above sea level via convection and advection, and the Himalaya range forms a 2500 km long, 8 km high complex topographic barrier along the northern edge of the IGP (Singh et al., 2004; Dey and Di Girolamo, 2010; Gautam et al., 2011).Numerous studies have investigated the transport of pollutants from the IGP to the Himalayan foothills, the immediate source region for potential transport to the Tibetan Plateau (TP)

(Pant et al., 2006; Dumka et al., 2008; Komppula et al., 2009; Hyvärinen et al., 2009; Ram et al., 2010; Brun et al., 2011; Gautam et al., 2011; Srivastava et al., 2012). Further, a suite of studies involving satellite imagery (Ramanathan et al., 2007a, Brun et al., 2011), back trajectories (Lu et al., 2011), model calculations (Kopacz et al., 2011), ice core analyses (Lee et al., 2008, Kang et al., 2010), and measurements in the higher Himalaya (Bonasoni et al., 2010) strongly suggest that pollutants are efficiently transported from the IGP to the higher Himalaya and onto the Tibetan Plateau, especially during spring prior to the monsoon. Absorbing aerosols warm the atmosphere at high altitudes and, when deposited onto snow and ice surfaces, decrease albedo thereby substantially increasing the rate of glacial and snow melting (Kang et al., 2010). Model simulations (Qian et al., 2011) show that the absorbing aerosols change the surface radiative flux in the higher Himalaya and the TP by 5 to 25 W m^{-2} during the pre-monsoon months of April and May. The TP plays a vital role in regulating the regional climate due to its effect on the Asian summer monsoon (ASM) and the hydrologic cycle. The interrelated perturbations of the ABC on radiative transfer, air quality, the hydrologic cycle, and crop yields have important long-term implications for human health, food security, and economic activity over southern Asia. However, to date, there has been little observational research to directly demonstrate the role of mountain valleys in the transport of air pollutants from the IGP and the Himalayan foothills to higher elevations within and north of the Himalayan range.

In other studied mountain ranges, it is well known that flow patterns carry polluted air masses up valleys to higher elevations by providing a path of least resistance between tall mountains. In the European Alps, prevailing wind systems in the mountain river valleys funnel polluted air from peripheral source regions to high elevations in a phenomenon known as "Alpine Pumping" (Weissmann et al., 2005). Under fair weather conditions during daytime, the upslope winds are capable of transporting significant pollutants and moisture into the free troposphere (Henne et al., 2004). Relative to air over plains, the air within the valley heats and cools more quickly (Steinacker, 1984). The resultant differences in temperature create gradients in pressure and density, which in turn drive transport of air from the plains to higher-elevations during the daytime (Reiter and Tang 1984, Whiteman and Bian, 1998; Egger et al., 2000). Such direct evidence of a Himalayan mountain valley wind system and its role in pollution transport has yet to be observed. Here we present 2.5 years of measurements of BC, O_3, and associated meteorological data from one of the deepest trans-Himalayan valleys, the Kali-Gandaki Valley. We examine seasonal and diurnal patterns of BC and O_3, investigate potential episodes of enhanced pollution transport up-valley, and make a preliminary estimate of BC mass transport. In doing so, we seek to provide the first observational evidence of trans-Himalayan valleys acting as conduits for pollution transport from the IGP to the higher Himalaya.

2. Measurement Sites and Methods

2.1 Measurement Sites and Instrumentation

This paper presents data from an atmospheric measurement station in Jomsom (28.87° N, 83.73° E, 2900 m asl) within the core region of the KGV along with four other automated weather stations up and down the valley from Jomsom. With the exception of aerosol optical depth measured as part of AERONET (AErosol RObotic NETwork) (Xu et al., 2015), no pollution data from Jomsom have been previously reported previously. Here we report diurnal and seasonal trends in two

important SLCPs – BC and O_3 – to evaluate the role of trans-Himalayan valleys as pathways for the transport of polluted air from the IGP to the higher Himalaya.

The KGV is located in the Dhaulagiri zone of western Nepal (Fig. 1(a)). The KGV floor changes elevation from approximately 1100 m to 4000 m above sea level (asl) over a horizontal distance of 90 km (Fig. 1(b)). Passing between the two eight thousand meter peaks of Dhaulagiri and Annapurna, it forms one of the deepest valleys in the world. The valley is a narrow gorge at the lower end and opens up into a wider, arid basin (Fig. 1(b)) with a maximum width of approximately one kilometer. The orientation of KGV varies from the entrance to the exit. The general orientation of the valley is from SW (the mouth of the valley) to NE (the head of the valley) (Fig. 1). Approximately 13,000 inhabitants in several small settlements sparsely populate the valley. Emission sources within the valley include biofuel combustion for cooking and fossil-fuel combustion by off-road vehicles. There is an airport in Jomsom which operates only in the morning as narrow valley width and high up-valley wind speeds make it dangerous for small aircraft to land at other times. A total of 5245 vehicles have been registered in Dhaulagiri Zone since 2008, but most are based in the southern towns of Kusma, Baglung, and Beni, below 1 km altitude, at the lowest left corner of the map in Figure 1(b) (DOTM, 2016).

The atmospheric observatory at Jomsom (JSM_STA) is equipped with instruments to measure BC, O_3, and meteorology (Figure 2). The observatory is located on the southeast corner of a plateau jutting out from an east-facing slope about 100 m above the valley floor and with no major obstructions either up or down the valley. Equivalent black carbon (hereafter referred to as BC) was measured with a Thermo Multiangle Absorption photometer (MAAP), model 5012 that uses a multi-angle photometer to analyze the modification of radiation fields – as caused by deposited particles that entered through a straight, vertical inlet line – in the forward and back hemisphere of a glass-fiber filter (GF-10). MAAP was operated at a flow rate of 20 L min^{-1}, measuring BC at 1-minute frequency. We note that Hyvärinen (2013) illustrates the artifact in MAAP measurements in environments with high aerosol loading with an underestimation of concentration above 9 µg m^{-3}. Since the median monthly concentrations for the duration of the measurement were less than 1µg m^{-3} and 90th percentile below 2 µg m^{-3} (and therefore below this threshold), MAAP corrections were not applied. O_3 was measured with a 2B Tech model 205 via the attenuation of ultraviolet light at 254 nm passing through a 15 cm long absorption cell fitted with quartz windows. The instrument was operated at a flow rate of 1.8 L min^{-1}. For instrument calibration, the BC instrument performed an automatic span and zero checks every 24 hours while zero checks on the O_3 instrument were performed every 7 days. Wind speed and direction were measured by an automated weather station installed on a ridge 900 m (JSM_2) above the sampling site for BC and O_3.

2.2 Data summary

The observatory operated from January 2013 through July 2015, but periodic power disruptions caused occasional data gaps (Table 1). Unless otherwise noted, data reported herein correspond to periods when BC, O_3, and meteorological data were available simultaneously. Data are binned by season as follows: monsoon (July-September), post-monsoon (October-

February) and pre-monsoon (March-June). Times correspond to Nepal's local time (LT) (UTC + 5.75 h). From March to May 2015, four additional automated weather stations were operated along a transect roughly 10 meters above and in the center of the valley floor where wind speeds are typically the highest: near the entrance of the valley at Lete (LET), within the core at Marpha (MPH) and Jomsom (JSM_2), and near the valley exit at Eklobhatti (EKL) (Fig. 1b). Power outages, instrument malfunctions, and a major earthquake in Nepal on April 25th, 2015 (and its aftershocks) limited the duration of records at all sites. However, between 1st and 14th May, all stations operated simultaneously and the resulting data provide information with which to evaluate diurnal variability of wind fields along the valley.

BC, O_3, and meteorological data were averaged over 10 minute intervals. Up-valley (southwesterly) flows are defined as between 35° and 55° while down-valley (northeasterly) flows include data between 215° and 235°. Data for all days for which complete data were available over entire 24-hour periods were binned by season. The statistical significance of differences between up-valley and down-valley flow conditions during different seasons were evaluated using the non-parametric Kruskal Wallis and Mann-Whitney tests.

To normalize for the influence of day-to-day variability in absolute concentrations, relative diurnal variability in O_3 and BC concentrations measured during a given month were normalized to a common scale ranging from 0 to 1 (see e.g., Sander et al., 2003; Fischer et al., 2006). Normalized BC values for month *m* were calculated as:

$$BC_{n,t} = \frac{BC_t - \min BC_m}{\max BC_m - \min BC_m}$$

where BC_t is the BC concentration at time *t* in the month *m*, and maxBC_m and minBC_m are the maximum and minimum BC concentrations observed during month *m*. The normalized data were then binned into twenty-four, hourly increments. These calculations were repeated for O_3.

2.3 Preliminary flux estimates

Up-valley and down-valley BC fluxes were calculated separately and determined using wind direction measurements. Instantaneous flux at time *t* was calculated as:

$$j_t = BC_t ws_t$$

where BC_t is the BC concentration (mg BC m^{-3}) at time *t* and ws_t is the wind speed (m hr^{-1}) at time *t*. From this, net daily mass transport (M_d) for day *d* was estimated as:

$$M_d = A\left(\sum\left(\frac{1}{6}j_{t,up}\right) - \sum\left(\frac{1}{6}j_{t,down}\right)\right)$$

where *A* is the cross-sectional area of the valley at Jomsom (1.41×10^6 m^2), $j_{t,up}$ and $j_{t,down}$ are the instantaneous up-valley and down-valley fluxes, respectively, occurring during day *d*, and the factor of 1/6 is the length of each time step in hours (i.e.,

10 minutes divided by 60 minutes). The cross-sectional area was estimated as a trapezoid with a height of 800 m (the difference in elevation between the two Jomsom stations) and cross-valley distances of 800 m (at JSM_1) and 2720 m (at JSM_2). The average of these two cross-valley distances (1760 m) multiplied by the height (800 m) yields the cross-sectional area of 1.41×10^6 m^2.

If we assume that (1) the polluted boundary layer within the valley at Jomsom is 800 m deep (i.e., the approximate elevational difference between the two AWS sites at Jomsom), (2) BC within the polluted boundary layer is well mixed, and (3) wind velocities do not vary significantly with altitude through the polluted layer, the mass flux BC through a vertical plane across the valley can be estimated. Supplementary Figure 1 shows that JSM_2 is well within the polluted haze layer during daytime/upvalley flows and that some BC is almost certainly transported above 800 m elevation. In this way we ensure that our estimates are conservative. The long lifetime of particulate BC against deposition (several days to a week or more) coupled with turbulent flow within the valley supports the assumption that BC is well mixed. Supplementary figure 2 shows that the potential temperature (theta) gradient is less than zero between JSM_1 and JSM_2 which illustrates that the air within the valley is unstable. In addition, Egger et al. (2000) used theodolite measurements to demonstrate uniform wind speeds within the bottom 1000m above the KGV floor at Jomsom and other locations. While we observed differences in wind speed of ~5 m s^{-1} between the two Jomsom stations during the limited times when data were available from both, we were unable to determine whether this pattern persisted throughout the year. These data limitations also prevented us from a more in-depth assessment of potential nighttime decoupling. For these reasons, our only option was to follow the findings of Egger et al. (2000) and assign the wind speed at JSM_2 to the entire flux plane.

3. Results and Discussion

3.1 Evolution of local wind system in the KGV

An understanding of the local wind regime is essential for analyzing pollution transport through mountain valleys. Measurements from JSM_2 show the diurnal evolution of wind at Jomsom in each season. All data collected were used to analyze the diurnal pattern of wind at Jomsom (Fig. 3a, 3b, 3c). Wind roses illustrate the temporal evolution of up- and down-valley flows at JSM_2 for each season. At JSM_2, up-valley flows are southwesterly and dominant during daytime, with peak velocities above 15 m s^{-1} between 0900 LT to 1800 LT. Wind velocities decreased substantially after 1800 LT, with variable wind direction until midnight, followed by northeasterly winds (during pre- and post-monsoon seasons (Fig. 3a and 3c)). The wind patterns during monsoon appear strongly influenced by the monsoon anticyclone; this observation is in agreement with wind direction measurements from other Himalayan valleys (Bonasoni et al., 2010; Ueno et al., 2008) (Fig. 5b). Although wind velocities at JSM_2 varied over the year, non-monsoon months exhibited similar diurnal patterns that evolved seasonally as a function of sunrise and sunset (Fig. 3a, 3b, 3c), characteristics which were exhibited in the monsoon season. As discussed below, this alternating pattern in wind direction from strong daytime flows to weak nighttime flows during dry months results in a net transport of pollutants up the valley.

Our measurements at the four AWS stations on the valley floor illustrate the evolution of surface wind velocities along the length of the KGV (Supplementary Figure 3). In general, wind speeds along the valley floor were strongest within the core of the valley at MPH, JSM_1 and JSM_2 and were lower in the entrance (LET) and exit (EKL) regions (Supplementary Figure 3). The duration of strong wind speeds within the valley during daytime is consistent with the hypothesis that wind patterns are modulated by the pressure gradient created as a result of differential heating of the arid valley floor relative to the mouth of the valley (Egger et al, 2000). In addition, comparison of measurements at JSM_1 and JSM_2 (Fig. 3a, 3b, 3c and Supplementary Figure 3) provided information regarding vertical variability in wind speed. Velocities at the higher elevation site of JSM_2 were about 5 m s^{-1} and 3 m s^{-1} greater than those near the valley floor during daytime and nighttime, respectively. The two sites exhibited similar diurnal cycles with the exception of a relatively stronger northeasterly wind at JSM_2 from 0300 to 0900 LST.

3.2 Diurnal variability in BC and O_3

Based on median values, O_3 peaked during daytime and dropped to minimal levels before sunrise during all three study seasons (pre-monsoon, monsoon, and post-monsoon. However, in April 2013(pre-monsoon period) O_3 peaked in the late afternoon whereas in November 2014(post-monsoon), it peaked in the early afternoon. In addition, the normalized diurnal excursions were greater during the pre- and post-monsoon periods relative to the monsoon period – represented by August 2014. In contrast, BC concentrations increased rapidly in the early morning, decreased during late morning, and then rose again through the afternoon and early evening hours (Fig. 4). Relative diurnal variability was somewhat greater during post-monsoon relative to the pre-monsoon and monsoon periods. Across all seasons, the lower normalized distributions for BC relative to O_3 reflect infrequent periods of high BC concentrations.

Several factors likely contributed to differences in timing of the daily peaks in O_3 and BC concentrations. These include potentially different source regions for BC and O_3 precursors, the timing of the photochemical production and destruction of O_3, and contributions of O_3 and its precursors from non-combustion sources like stratospheric ozone and biogenic hydrocarbons from vegetation. The early morning BC peak during all seasons suggests contributions from the local combustion of biofuels for cooking and heating, which are most prevalent during early morning. The secondary peak in the afternoon and early evening occurs when the local anthropogenic emission sources are at a minimum in the KGV.

3.3 Seasonal variability in BC and O_3

All data generated during the measurement period were binned by month to evaluate the seasonal patterns of BC and O_3 (Fig. 5). In addition, individual months with the most complete data coverage during the pre-monsoon (April 2013), monsoon (August 2014), and post-monsoon (November 2014) seasons were selected to evaluate aspects of temporal variability in greater detail (Fig. 5). We divided the seasons into dry (pre-monsoon, post-monsoon) and wet (monsoon) seasons to understand the transport of pollutants via Himalayan valleys in the presence and absence of wet deposition processes. Based on median values, the highest concentrations of both species occurred during the months preceding the monsoon and the

lowest were during months of the monsoon. The significantly lower concentrations during the monsoon reflect the combined influences of synoptic easterly airflow that transports a cleaner marine air mass over the region, reduced agricultural residue burning (Sarangi et al., 2014), and more efficient aerosol removal via wet deposition (Dumka et al., 2010). In addition to possible active wet deposition of O_3 precursors during the monsoon season, increased cloudiness during monsoon may also reduce O_3 production (Lawrence and Lelieveld, 2010).

The post-monsoon timing of peak BC concentrations observed in previous studies performed in the IGP and Himalayan foothills (see e.g., Tripathi et al, 2005; 2007; Ramchandran et al., 2007; Putero et al, 2015) differs from our observations in the KGV, where we see heightened BC during the pre-monsoon season (Fig. 5). These findings are generally in agreement with other high altitude observations. For example, the Nepal Climate Observatory-Pyramid (NCO-P) station at the 5079 m asl in the Himalaya has also shown high seasonal differences for BC and O_3 between pre-monsoon (0.444 (±0.443) μg m^{-3} BC; 61 (±9) ppbv O_3) and monsoon (0.064 (±0.101) μg m^{-3} BC; 39 (±10) ppbv O_3) (Cristofanelli et al., 2010, Marinoni et al., 2013) (Table 2). Our results therefore indicate a lagged peak in BC and O_3 within the KGV and presumably other deep Himalayan valleys, as compared to sites within the IGP.

3.4 Local winds as drivers of BC and O_3 transport in the KGV

Figure 6 shows the time series of BC and O_3 during individual month in each season (April/pre-monsoon, August/monsoon, November/post-monsoon). For April, BC concentrations peaked at 0700 LST (Fig.6) when wind velocities were low (Fig.6). This peak occurred about an hour later in November, with both periods experiencing a decrease in BC over the rest of the morning as wind speeds increased and diluted local emissions (Fig.4). Thereafter, BC concentrations increased over the afternoon and early night, reaching secondary peaks near midnight LST in April and several hours earlier in November and August (Fig. 4 and6). Distinct morning and afternoon peaks in BC concentration are seen in the post-monsoon season when the up-valley wind speeds are relatively weaker than in pre-monsoon season (Fig. 4 and 6). The bimodal diurnal distribution of BC concentration in Jomsom is similar to that observed in Kathmandu (Putero et al. 2015) but unlike a singular late afternoon/evening peak seen at high elevation sites (Bonasoni et al., 2010) during non-monsoonal seasons. This illustrates that deep Himalayan valleys are susceptible to diurnal pollution similar to that of urban areas like Kathmandu. The morning peak in BC is most likely due to local pollutants (from household and morning aircraft traffic) in Jomsom and settlements downwind of Jomsom, while the afternoon peak is likely primarily associated with long range in addition to local pollutants. At the same time, O_3 exhibits a distinct minimum in the early morning with concentrations increasing towards an early afternoon peak – occurring well before BC's afternoon peak. The O_3 minimum in the morning further supports that the morning BC peak originates from local sources, as O_3 is only formed downwind of pollution sources. Further, the Jomsom station measuring BC and O_3 (JSM_STA) is located more than 100 m above the valley floor where the village of Jomsom sits. As such, we do not expect that local evening emissions would reach the stations at the cessation of up-valley flows and that evening drainage flows, following the valley floor would remove these local evening emissions down-valley.

Percentage distributions of up-valley and down-valley BC concentrations, fluxes, and net daily fluxes are depicted in Figure 7 and summarized in Supplementary Table 1. The differences in BC concentration between up-valley and down-valley flows are quite similar yet statistically significant for all seasons, with higher down-valley concentrations (Figure 7a). However, because wind velocities were relatively higher during up-valley daytime flow and the durations of up-valley were modestly longer than those of down-valley flow, the corresponding up-valley fluxes of BC during daytime were markedly and significantly greater than down-valley fluxes during all seasons (Fig. 7b). These results suggest an oscillatory movement of polluted air within the valley, where polluted air masses are pushed up-valley during daytime and retreat a shorter distance during nighttime. These differences between up-valley and down-valley fluxes yielded significant net daily up-valley fluxes of BC during all seasons (Fig. 7c). Because heating would have driven growth of the boundary layer and thus greater ventilation and dilution of pollutants during daytime relative to night, we infer that the calculated differences in up-valley versus down-valley fluxes correspond to lower limits for net BC fluxes.

Positive up-valley fluxes are consistent with an "alpine pumping" mechanism in the Himalayan valleys and thereby support the hypothesis that these valleys are important pathways for pollution transport. In addition, we estimate substantial net daily mass transport of BC up the valley during the pre-monsoon season: 1.05 kg day^{-1} (based on the average net daily flux) and 0.72 kg day^{-1} (based on the median net daily flux). While preliminary, these estimates provide the first semi-quantitative constraints on mass transport of BC from the IGP to the high Himalaya through deep valleys and, more generally, on the regional cycling of BC over southern Asia.

3.5 Evidence of regional transport episodes in valley concentration

Along with the regular diurnal and seasonal variability driven by local winds as described above, we also observed anomalous periods – lasting several days to more than a week – during which BC concentrations were significantly greater than the 90^{th} percentile for corresponding annual averages (Table 3). These extended periods of high BC at JSM_STA are evidence of large-scale transport from the IGP to the foothills in conjunction with local valley winds (Fig. 8). Elevated O_3 concentrations did not always accompany these long-duration periods of high BC concentrations above 90^{th} percentile. Different atmospheric lifetimes, chemical reactivity, source location, and sinks of BC and O_3 all may contribute to these differences in BC and O_3 concentrations detected in the valley. Table 3 reports the number of days in which O_3 concentration was above 90^{th} percentile within each episode.

We partitioned these episodes into three characteristic patterns based on the relative variability of BC. Pattern A was characterized as a fluctuating daily maximum in BC with peaks that repeatedly exceeded the 90^{th} percentile but with daily minima below the 90^{th} percentile (Fig. 8[Ia]). Pattern B was characterized by a steady buildup of BC concentration over the period of the regional transport episode, with peak BC concentrations over the 90^{th} percentile but without a low daily minimum (Figure 8b). Pattern C exhibited a combination of both Patterns A and B during a single regional episode (Figure 8c). A total of 34 regional episodes were identified from January 2013 through June 2015, 47% of which were categorized as

Pattern A, 32% as Pattern B, and 21% as Pattern C. The wind speeds at Jomsom during these transport episodes exhibited diurnal variability similar to those during other periods (Fig. 8 [II]). During the regional transport period in November 2014 (Pattern A), average daily BC concentration was 1.29 μg m^{-3} which is over the 75th percentile (0.88 μg m^{-3}) of the BC concentration for the measurement duration. The maximum daily concentration during the period was 3.04 μg m^{-3}. However, the corresponding average O_3 was only 28.07 ppbv, slightly below the average (29.48 ppbv) for the entire data set (Figure 8 [Ia]). The mean BC concentration during pattern B, one example of which occurred in May 2014, was 1.77 μg m^{-3} (Figure 8[Ib]). It was above the 90th percentile (1.49 μg m^{-3}) for entire measurement period while O_3 concentrations were at 49.71 ppbv, slightly below the 90th percentile (52.9 ppbv). One of the Pattern C- type transport episodes was identified in May 2013, when the average concentration was well above the 90th percentile for both BC (2.09 μg m^{-3}) and O_3 (57.49 ppbv) (Fig. 8 [Ic]). The diurnal wind pattern in the KGV was conserved during the Pattern A example, but a longer period of up-valley flows occurred during the examples for Patterns B and C (Fig. 8).

4. Conclusion

This study provides new in-situ observational evidence of the role of a major Himalayan valley as an important pathway for transporting air pollutants from the IGP to the higher Himalaya. We found that concentrations of BC and O_3 in the KGV exhibited systematic diurnal and seasonal variability. The diurnal pattern of BC concentrations during the pre- and post-monsoon seasons were modulated by the pulsed nature of up-valley and down-valley flows. Seasonally, pre-monsoon BC concentrations were higher than in post-monsoon season. We also found that morning and afternoon peaks in the post-monsoon season were more pronounced than those of pre-monsoon season, likely due to the relatively lower wind speeds during post-monsoon. Significant positive up-valley fluxes of BC were measured during all seasons and preliminary flux estimates (which require a more robust estimate in future work) show the efficiency and magnitude of pollutant transport up the valley. During episodes of regional pollution over the IGP, relatively higher concentrations of BC and O_3 were also measured in the KGV.

The frequency and magnitude of pollution events highlighted in the paper need to be studied for a longer period in order to understand the associated interannual variability. In addition, future work should focus on understanding the vertical and horizontal distribution of particulate matter and ozone in the Himalayan region, and their impacts on the radiative budget, the ASM and regional climate.

Acknowledgments.

We would like to acknowledge our field assistant in Nepal, Buddhi Lamichhane who helped us in various stages of the study, as well as the logistic and administrative support and internet at the Jomsom station provided by Nepal Wireless. Financial support was provided by the National Aeronautics and Space Administration NNX12AC60G, and additional field support was provided by ICIMOD's Atmosphere Initiative. The authors are very thankful for comments from William Keene, Jennie Moody and Kyle Davis.

References.

Andreae, M. O. and Crutzen, P. J.: Atmospheric Aerosols: Biogeochemical Sources and Role in Atmospheric Chemistry, Science, 1052-1058, 1997.

Auffhammer, M., Ramanathan, V. and Vincent, J. R.: Integrated model shows that atmospheric brown clouds and greenhouse gases have reduced rice harvests in India, *PNAS* 10.1073/pnas.0609584104, 2006.

Bonasoni, P., Laj, P., Marinoni, A., Sprenger, M., Angelini, F., Ar- duini, J., Bonafe, U., Calzolari, F., Colombo, T., Decesari, S., Di Biagio, C., di Sarra, A. G., Evangelisti, F., Duchi, R., Facchini, M. C., Fuzzi, S., Gobbi, G. P., Maione, M., Panday, A., Roccato, F., Sellegri, K., Venzac, H., Verza, G. P., Villani, P., Vuillermoz, E., and Cristofanelli, P.: Atmospheric Brown Clouds in the Himalayas: first two years of continuous observations at the Nepal Climate Observatory-Pyramid (5079 m*), Atmos. Chem. Phys.*, 10, 7515–7531, doi:10.5194/acp-10-7515-2010, 2010.

Bond, T., Doherty, S., Fahey, D., Forster, P., Berntsen, T., DeAngelo, B., Flanner, M., Ghan, S., Kärcher, B., and Koch, D.: Bounding the role of black carbon in the climate system: A scientific assessment, J. Geophys. Res.-Atmos., 118, 5380–5552, doi:10.1002/jgrd.50171, 2013.

Brun, J., Shrestha, P., Barros, A., P.: Mapping aerosol intrusion in Himalayan valleys using the Moderate Resolution Imaging Spectroradiometer (MODIS) and Cloud Aerosol Lidar and Infrared Pathfinder Satellite Observation (CALIPSO), *Atmos. Env*., 45 (2011) 6382-6392, 2011.

Cristofanelli, P., Bracci, A., Sprenger, M., Marinoni, A., Bonafè, U., Calzolari, F., Duchi, R., Laj, P., Pichon, J. M., Roccato, F., Venzac, H., Vuillermoz, E., and Bonasoni, P.: Tropospheric ozone variations at the Nepal Climate Observatory-Pyramid (Himalayas, 5079 m a.s.l.) and influence of deep stratospheric intrusion events, Atmos. Chem. Phys., 10, 6537–6549, doi:10.5194/acp-10-6537-2010, 2010.

Dey, S., and Di Girolamo, L.: A climatology of aerosol optical and microphysical properties over the Indian subcontinent from 9 yr (2000–2008) of Multiangle Imaging Spectroradiometer (MISR) data, *J. Geophys. Res.*, 115, D15204, doi:10.1029/2009JD013395, 2010.

Decesari, S., Facchini, M.C., Carbone, C., Giulianelli, L., Rinaldi, M., Finessi, E., Fuzzi, S., Marinoni, A., Cristofanelli, P., Duchi, R., Bonasoni, P., Vuillermoz, E., Cozic, J., Jaffrezo, J., L., Laj, P.: Chemical composition of PM_{10} and PM_1 at the high-altitude Himalayan station Nepal Climate Observatory-Pyramid (NCO-P) (5079 m a.s.l.), *Atmos. Chem. Phys.*, 10: 4583–4596, 2010.

DOTM-Vehicle data zonal wise till 2072 baishakh, Government of Nepal, Department of Transportation Management (http://www.dotm.gov.np/uploads/files/Vehicle-data-zonal-wise-till-2072-baishakh.pdf) accessed March 26th, 2016.

Dumka, U., C., Krishna Moorthy, K., Satheesh, S., K., Sagar, R., Pant, P.: Short-period modulations in aerosol optical depths over the central Himalayas: role of mesoscale processes, *J. Appl. Meteor. Climatol.*, doi: 10.1175/2007JAMC1638.1, 2008.

Dumka, U., C., Moorthy, K., K., Kumar, R., Hegde, P., Sagar, R., Pant, P., Singh, N., Babu, S.: Characteristics of aerosol

black carbon mass concentration over the high altitude location in the central Himalayas from multi-year observations. *Atmos. Res.*, 96, 510-521 2010.

Egger, J., Bajracharya, S., Egger, U., Heinrich, R., Reuder, J., Shakya, P., Wendt, H., and Wirth, V.: Diurnal winds in the Himalayan Kali Gandaki valley. Part I: observations, *Mon. Weather Rev.*, 128, 1106-1122, 2000.

Egger, J., Bajracharya, S., Egger, U., Heinrich, R., Kolb, P., Lammlein, S., Mech, M., Reuder, J., Schaper, W., Shakya, P., Schween, J. and Wendt, H.: Diurnal winds in the Himalayan Kali Gandaki valley. Part III:remotely piloted aircraft soundings, *Mon. Weather Rev*., 130, 2042-2058, 2002.

Engling, G., and Galencser, A.: Atmospheric brown clouds: from local air pollution to climate change, *Elements*, 6, 223-228, 2010.

Fadnavis, S., Semeniuk, K., Pozzoli, L., Schultz, M. G., Ghude, S. D., Das, S., and Kakatkar, R.: Transport of aerosols into the UTLS and their impact on the Asian monsoon region as seen in a global model simulation, Atmos. Chem. Phys., 13, 8771–8786, 2013.

Fischer, E., Pszenny, A., Keene, W., Maben, J., Smith, A., Stohl, A., Talbot R.: Nitric acid phase partitioning and cycling in the New England coastal atmosphere, J. Geophys. Res., 111, D23S09, doi:10.1029/2006JD007328, 2006.

Flanner, M. G., Zender, C. S. , Hess, P. G., Mahowald, N. M., Painter, T. H., Ramanathan, V., Rasch , P. J.: Springtime warming and reduced snow cover from carbonaceous particles, Atmos. Chem. Phys., 9 (7), 2481- 2497, doi: 10.5194/acp-9-2481-2009, 2009.

Gautam, R., Hsu, N., C., Tsay, S., C., Lau, K., M., Holben, B., Bell, S., Smirnov, A., Li, C., Hansell, R., Ji, Q., S. Payra, S., Aryal, D., Kayastha, R., K. M. Kim, K., M. : Accumulation of aerosols over the Indo-Gangetic plains and southern slopes of the Himalayas: distribution, properties and radiative effects during the 2009 pre-monsoon season, *Atmos. Chem. Phys.*, 11, 12841–12863, 2011

Gustafsson, O., Kruså, M., Zencak, Z., Sheesley, R., J., Granat, L., Engström,E., Praveen, P., S., Rao, P., S., P., Leck, C., Rodhe, H.: Brown Clouds over South Asia: Biomass or Fossil Fuel Combustion?, *Science*, 323, 495-498, 2009.

Henne, S., Furger, M., Nyeki, S., Steinbacher, M., Neininger, B., de Wekker, S.F.J, Dommen, J., Spichtinger, N., A. Stohl, A. and Prevót A. S. H.: Quantification of topographic venting of boundary layer air to the free troposphere, *Atmos. Chem. Phys*., 4, 497–509, 2004.

Hyvärinen, A., P., Lihavainen, H., Komppula, M., Sharma, V., P., Kerminen, V., M., Panwar, T., S., Viisanen, Y.: Continuous measurements of optical properties of atmospheric aerosols in Mukteshwar, Northern India, *J. Geophys. Res.*, 114: D08207, doi: 10.1029/2008JD011489, 2009.

Hyvarinen, A., -P., Vakkari, V., Laakso, L., R. K. Hooda, R., K., Sharma, V., P., Panwar, T., S., Beukes, J., P., van Zyl, P.,

G., M. Josipovic, M., Garland, R. M., Andreae, M. O., Poschl, U., Petzold, A. : Correction for a measurement artifact of the Multi-Angle Absorption Photometer (MAAP) at high black carbon mass concentration levels, *Atmos. Meas. Tech.*, 6, 81–90, 2013

Jacobson, M., Z.: Strong radiative heating due to the mixing state of black carbon in atmospheric aerosols, *Nature*, 409, 695-697, 2001.

Janssen, Nicole A. H., Hoek, G., Simic-Lawson, M., Fischer, P., van Bree, L., Brink, H., Keuken, M., Atkinson, R. W., Anderson, H. R., Brunekreef, B., and Cassee, F. R.: Black carbon as an additional indicator of the adverse health effects of airborne particles compared with PM_{10} and $PM_{2.5}$, *Environ. health persp.* 119 (12), 1691-1698, 2011.

Kang, S., Xu, Y., You, Q., Flugel, W-A., Pepin, N. and Yao, T. review of Climate and cryospheric change in the Tibetan Plateau, *Environ. Res. Lett.* 5(1), 015101, 2010.

Kaufman, Y. J., Tanré, D., and Boucher, O.: A satellite view of aerosols in the climate system, *Nature*, 419, 215–223, 2002.

Koch, D., Schulz, M., Kinne, S., McNaughton, C., Spackman, J.R., Balkanski, Y., Bauer, S., Berntsen, T., Bond, T.C., Boucher, O., Chin, M., Clarke, A., De Luca, N., Dentener, F., Diehl, T., Dubovik, O., Easter, R., Farey, D.W., Feichter, J., Fillmore, D., Freitag, S., Ghan, S., Ginoux, P., Gong, S., Horowitz, L., Iversen, T., Kirkevåg, A., Klimont, Z., Kondo, Y., Krol, M., Liu, X., Miller, R., Montanaro, V., Moteki, N., Myhre, G., Penner, J.E., Perlwitz, J., Pitari, G., Reddy, S., Sahu, L., Sakamoto, H., Schuster, G., Schwarz, J.P., Seland Ø, Stier P., Takegawa, N., Takemura, T., Textor, C., van Aardenne, J.A., Zhao, Y.: Evaluation of black carbon esti- mations in global aerosol models. Atmospheric Chemistry and Physics 9, 9001e9026.Komppula, M., Lihavainen, H., A.-P. Hyvärinen,A., -P., Kerminen, V., –M., Panwar, T., S., Sharma, V., P., Viisanen, Y.: Physical properties of aerosol particles at a Himalayan background site in India, *J. Geophys. Res.*, 112, doi:10.1029/2008JD011007, 2009.

Kopacz, M., Mauzerall,D., L., Wang, J.,Leibensperger, E., M., Henze, D., K., and K. Singh, K.: Origin and radiative forcing of black carbon transported to the Himalayas and Tibetan Plateau, *Atmos. Chem. Phys.*, 11, 2837–2852, 2011.

Krupnick, A., J., Harrington, W., Ostro, B.: Ambient ozone and acute health effects: Evidence from daily data, *J. Environ. Econ. Manag.*, 18(1), 1-18, 1990.

Lau, K., M., Kim, M., K., Kim, K., M.: Asian summer monsoon anomalies induced by aerosol direct forcing: The role of the Tibetan Plateau, *Climate Dynamics*, 26, 855–864, 2006.

Lawrence, M. G. and Lelieveld, J.: Atmospheric pollutant outflow from southern Asia: a review, *Atmos. Chem. Phys.*, 10, 11017–11096, doi:10.5194/acp-10-11017-2010, 2010.

Lee K, Soon DH, Shugui H, Sungmin, Xiang Q, Jaiwen R, Yapping L, Rosmann KJRR, Barbante C, Bourton CF.: Atmospheric pollution of trace elements in the remote high-altitude atmosphere in Central Asia as recorded in snow from Mt Qomolangma (Everest) of the Himalayas, *Sci. Tot. Environ.* 404, 171-181, 2008.

Lu, Z., Zhang, Q., and Streets, D., G.: Sulfur dioxide and primary carbonaceous aerosol emissions in China and India, 1996–2010, *Atmos. Chem. Phys.*, 11, 9839-9864, 2011.

Ma, J., Chen, Y., Wang, W., Yan, P., Liu, H.,Yang, S., Hu, Z., and Lelieveld, J.: Strong air pollution causes widespread

haze-clouds over China, *J. Geophys. Res.*, 115, D18204, 2010.

Marinoni, A., Cristofanelli, P., Laj, P., Duchi., R., Calzolari, F., Decesari, S., Sellegri, K., Vuillermoz, E., Verza, P., Villani, P., Bonasoni, P. Aerosol mass and black carbon concentrations, a two year record at NCO-P (5079 m, Southern Himalayas), *Atmos., Chem. Phys.*, 10, 8551-8562, 2010.

Marinoni, A., Cristofanelli, P., Laj, P., Duchi., R., Putero, D., Calzolari, F., Landi., T., C., Vuillermoz, E., Maione, M., Bonasoni, P.: High black carbon and ozone concentrations during pollution transport in the Himalayas: Five years of continuous observations at NCO-P global GAW station, *J. Environ. Sci.*, 25(8) 1618–1625, 2013.

Menon, S., Hansen, J., Nazarenko, L. and Yunfeng, L.: Climate Effects of Black Carbon Aerosols in Aerosols in China and India, *Science*, 297, 2250-2253, 2002.

Pant, P., Hegde, P., Dumka, U., C., Sagar, R., Satheesh, S., K., Krishna Moorthy, K., Saha, A., Srivastava, M., K.: Aerosol characteristics at high-altitude location in central Himalayas: optical properties and radiatuve forcing, *J. Geophys. Res.*, doi:10.1029/2005JD006768, 2006.

Piketh, S. J., Annegarn, H., J., and Tyson, P., D.: Lower tropospheric aerosol loadings over South Africa: The relative contribution of aeolian dust, industrial emissions, and biomass burning, *J. Geophys. Res.*, 104(D1), 1597–1607, 1999.

Qian, Y., Flanner, M. G., Leung, L. R., and Wang, W.: Sensitivity studies on the impacts of Tibetan Plateau snowpack pollution on the Asian hydrological cycle and monsoon climate, At- mos. Chem. Phys., 11, 1929–1948, doi:10.5194/acp-11-1929- 2011, 2011.

Raatikainen, T., Hyvärinen, A.-P., Hatakka, J., Panwar, T., S., Hooda, R., K., Sharma, V., P., Lihavainen, H.: The effect of boundary layer dynamics on aerosol properties at the Indo-Gangetic plains and at the foothills of the Himalayas, *Atmos. Env.*, 89, 548-555, 2014.

Raatikainen, T., Brus, D., Hooda, R., K., Hyvärinen, A.-P., Asmi, E., Sharma, V., P., Arola, A., Lihavainen, H.: Size-selected black carbon mass distributions and mixing state in polluted and clean environments of northern India, *Atmos. Chem. Phys.* 17, 371-383, 2017.

Ram, K., Sarin, M., M. and Hegde, P.: Long-term record of aerosol optical properties and chemical composition from a high-altitude site (Manora Peak) in central Himalaya, *Atmos. Chem. Phys.*, 10: 11791–11803, 2010.

Ramanathan, V., and Carmichael, G.: Global and regional climate changes due to black carbon, *Nat. Geosci.*, 1(4), 221–227, 2008.

Ramanathan, V., Chung, C., Kim, D., Bettge, T., Buja, L., Kiehl, J., T., Washington, W., M., Fu, Q., Sikka, D., R., and Wild, M.: Atmospheric brown clouds: Impacts on South Asian climate and hydrological cycle, *PNAS*, 102(15), 5326-5333, 2005.

Ramanathan, V. and Crutzen, P. J.: New Directions: Atmospheric Brown “Clouds”, Atmos. Env., 37, 4033-4035, 2003.

Ramanathan, V., Ramana, V., M., Roberts, G., Kim, D., Corrigan, C., Chung, C., Winker, D.: Warming trends in Asia amplified by brown cloud solar absorption, *Nature*, 448(2), 575-578, 2007a.

Ramanathan, V., Li, F., Ramana, M.V., Praveen, P.S., Kim, D., Corrigan, C.E., Nguyen, H., Stone, E.A., Schauer, J.J.,

Carmichael, G.R., Adhikary, B., Yoon, S.C.: Atmospheric Brown Clouds: Hemispherical and Regional Variations in Long-Range Transport, Absorption, and Radiative Forcing, *J. Geophys. Res.*, 112, D22821, 2007b.

Reche, C., Querol, X., Alastuey, A., Viana, M., Pey, J., Moreno, T., Rodríguez, S., González, Y., Fernández-Camacho, R., De La Campa, A. M, Sálnchez,De La Rosa, J., Dall'Osto, M., Prévôt, A. S H, Hueglin, C., Harrison, R. M., Quincey, P.: New considerations for PM, Black Carbon and particle number concentration for air quality monitoring across different European cities, *Atmos. Chem. Phys.*, 11, 6207–6227, 2011.

Reddy, M.S. and Venkataraman, C.: Inventory of Aerosol and Sulphur Dioxide Emissions from India: II – Biomass Combustion, Atmos. Envir., 36 (4), 699-712, 2002.

Reiter, E. R., and Tang, M.: Plateau effects on diurnal circulation patterns. *Mon. Wea. Rev*., 112, 638–651, 1984.

Sander, R., Keene, W. C., Pszenny, A. A. P., Arimoto, R., Ayers, G. P., Baboukas, V., Chainey, J. M. Crutzen, P. J., Duce, R. A., Hönninger, G., Huebert, B. J., Maenhaut, W., Mihalopoulos, N., Turekian, V. C., van Dingenen, R.: Inorganic bromine in the marine boundary layer: A critical review, Atmos. Chem. Phys, 3, 1301-1336, 2003.

Sarangi, T., Naja, M., Ohja, N., Kumar, R., Lal, S., Venkataramani, S., Kumar, A., Sagar, R., Chandola, H., C.: First simultaneous measurements of ozone, CO and NO_y at a high-altitude regional representative site in the central Himalayas, *JGR*, 119(3), 1592-1611, 2014).

Singh R. P., Dey, S., Tripathi, S. N., Tare, V., and Holben, B.: Variability of aerosol parameters over Kanpur, northern India, *J. Geophys. Res.*, 109, D23206, doi:10.1029/2004JD004966, 2004.

Sreekanth, V., Niranjan, K., Madhavan, B. L.: Radiative forcing of Black Carbon over Eastern India, *Geophys. Res. Lett.*, 34(L17818), doi: 10.1029/2007GL030377, 2007.

Srivastava, A., K., Singh, S., Pant, P. and Dumka, U., C. : Characteristics of black carbon over Delhi and Manora peak - A comparative study, *Atmos. Sci. Lett.*,13: 223–230, 2012.

Stein, A.F., Draxler, R.R, Rolph, G.D., Stunder, B.J.B., Cohen, M.D., and Ngan, F., (2015). NOAA's HYSPLIT atmospheric transport and dispersion modeling system, Bull. Amer. Meteor. Soc., 96, 2059-2077, http://dx.doi.org/10.1175/BAMS-D-14-00110.1, 2015.

Steinacker, R.: Area–height distribution of a valley and its relation to the valley wind, Beitr. Phys. Atmos., 57, 64–71, 1984.

Streets, D. G., Bond, T. C., Carmichael, G. R., Fernandes, S. D., Fu, Q., He, D., Klimont, Z., Nelson, S. M., Tsai, N. Y., Wang, M. Q., Woo, J. H., and Yarber, K. F.: An inventory of gaseous and primary aerosol emissions in Asia in the year 2000, J. Geophys. Res.-Atmos., 108, 8809, doi:10.1029/2002JD003093, 2003.

The Royal Society, 2008. Ground-level ozone in the 21st century: future trends, impacts and policy implications. Science policy report 15/08. The Royal Society, London.

Tripathi, S. N., Dey, S., Tare, V., Satheesh, S. K.: Aerosol black carbon radiative forcing at an industrial city in northern India. Geophys. Res. Lett. 32 (L08802). doi:10.1029/2005GL022515, 2005.

Tripathi, S. N., Srivastava, A. K., Dey, S., Satheesh, S. K., Moorthy, K. K.: The vertical profile of atmospheric heating rate of black carbon aerosols at Kanpur in northern India. Atmos. Env.41: 6909–6915, 2007.

Ueno, K., Toyotsu, K., Bertolani, L., and Tartari, G.: Stepwise onset of Monsoon Weather Observed in the Nepal Himalayas, Mon. Weather Rev., 136(7), 2507–2522, 2008.

Vasilyev, O. B., Contreras, A., L., Velazquez, A., M., Fabi, R., P., Ivlev, L., S., Kovalenko, A., P., Vasilyev, A., V., Jukov, V., M., and Welch, R., M.: Spectral optical properties of the polluted atmosphere of Mexico City (spring-summer 1992), *J. Geophys. Res.*, 100(D12), 26027–26044, 1995.

Weissmann, M., Braun, A. F. J., Gantner, A., L., Mayr, A., G., J.,Rahm, A., S., Reitebuch, A., O. :The Alpine Mountain–Plain Circulation: Airborne Doppler Lidar Measurements and Numerical Simulations, *Mon. Weather Rev.*, 133,(11), 3095-3109, 2005.

Whiteman, C. D., and Bian X.: Use of radar profiler data to investigate large-scale thermally driven flows into the Rocky Mountains, *Proc. Fourth Int. Symp. on Tropospheric Profiling: Needs and Technologies*, Snowmass, CO, 1998.

Xu, C., Ma, Y. M., You, C., and Zhu, Z. K.: The regional distribution characteristics of aerosol optical depth over the Tibetan Plateau, *Atmos. Chem. Phys*., 15, 12065–12078, 2015.

Yasunari, T. J., Bonasoni, P., Laj, P., Fujita, K., Vuillermoz, E., Marinoni, A., Cristofanelli, P., Duchi, R., Tartari, G., and Lau, K.-M.: Estimated impact of black carbon deposition during pre- monsoon season from Nepal Climate Observatory - Pyramid data and snow albedo changes over Himalayan glaciers, Atmos. Chem. Phys., 10, 6603–6615, doi:10.5194/acp-10-6603-2010, 2010.

Zangl, G., Egger, J., and Wirth, V.: Diurnal Winds in the Himalayan Kali Gandaki Valley. Part II: Modeling, *Mon. Weather Rev*., 129, 1062-1080, 2000.

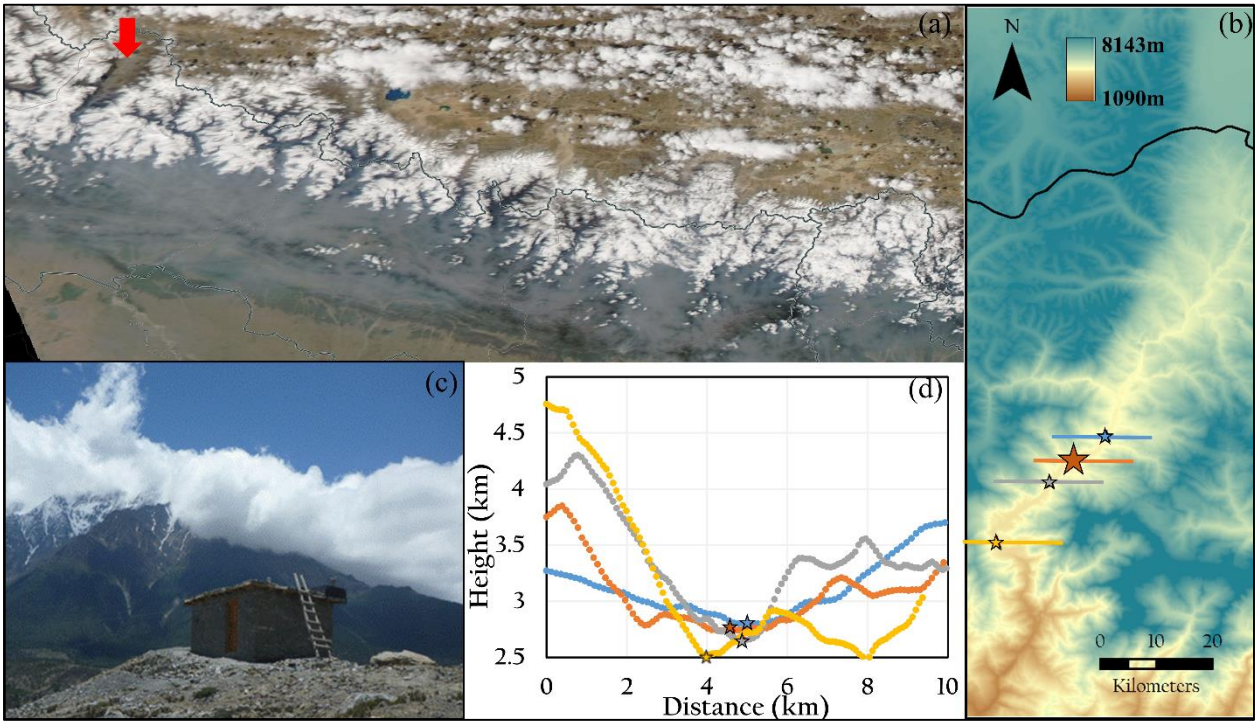

Figure 1. (a) NASA Worldview image from November 4th , 2014 depicting thick haze intruding the Himalayan foothills with red arrow over the KGV. (b) Expanded scale of the KGV showing locations of LET near the entrance of the valley (yellow star); MPH in the core region (gray star); the JSM_STA sampling station for BC and O_3 and the two associated AWS sites (JSM_1 and JSM_2) in the core region (orange star); and EKL near the exit (blue star). (c) The atmospheric observatory at Jomsom (JSM_STA). (d) Cross-sectional elevation profile at the indicated locations.

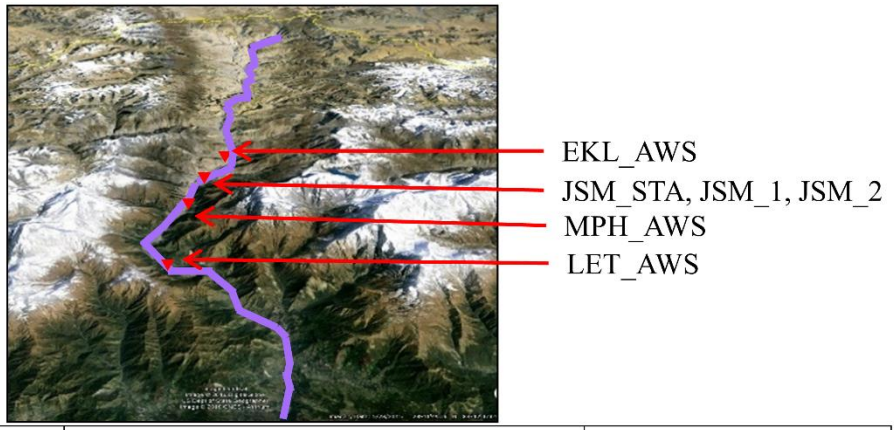

Station	Location	Elevation	Instrument(parameters measured)	Measurement period
JSM_STA	28.87N, 83.73E	2850m	Thermo BC MAAP–Model 5012 (Black carbon)	Jan 2013 – July 2015
			2B Tech Ozone instrument–Model 205 (Ozone)	Jan 2013 – July 2015
JSM_1	28.87N, 83.73E	2800m	DAVIS–Model Vantage Pro 2 (WD, WS, T, RH, DP)	Mar – May 2015
JSM_2	28.87N, 83.73E	3700m	NexSens–Model Vaisala WXT520 (WD, WS, T, RH, DP, Precip, Solar rad)	Jan 2013 – July 2015
LET_AWS	28.93N, 83.35E	2500m	Nexsens–ModelVaisala WXT520 (WD, WS, T, RH, DP, Precip, Solar rad)	Mar – May 2015
MPH_AWS	28.44N, 83.41E	2665m	HOBO–Model AWS U–30 (WD, WS, T)	Mar – May 2015
EKL_AWS	28.49N, 83.46E	2804m	NexSens–ModelVaisala WXT520 (WD, WS, T, RH, DP, Precip, Solar rad)	Mar – May 2015

Figure 2. The valley floor of KGV is shown in purple along with details pertaining to measurement sites, the installed instruments and measurement period.

Table 1. Data timeline for JSM_2 AWS, BC and O_3 measurements in Jomsom. Green indicates complete data, blue is with few data points missing, yellow is more than 15 days data, orange is less than 15 days and blank is no data.

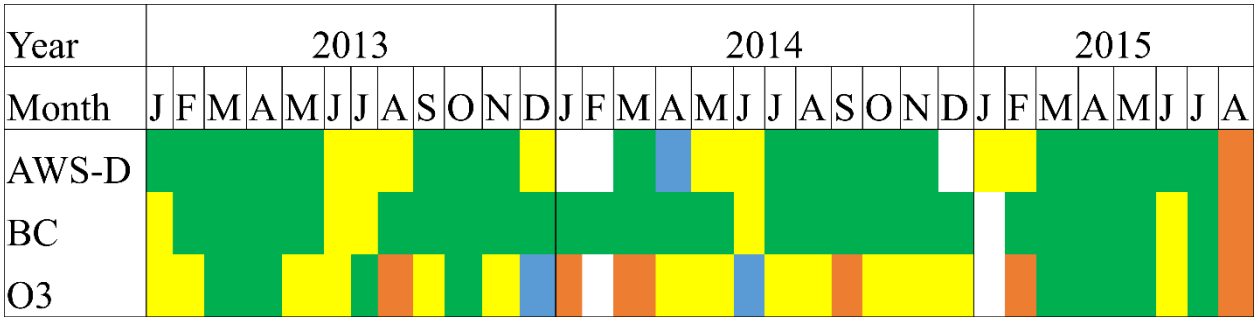

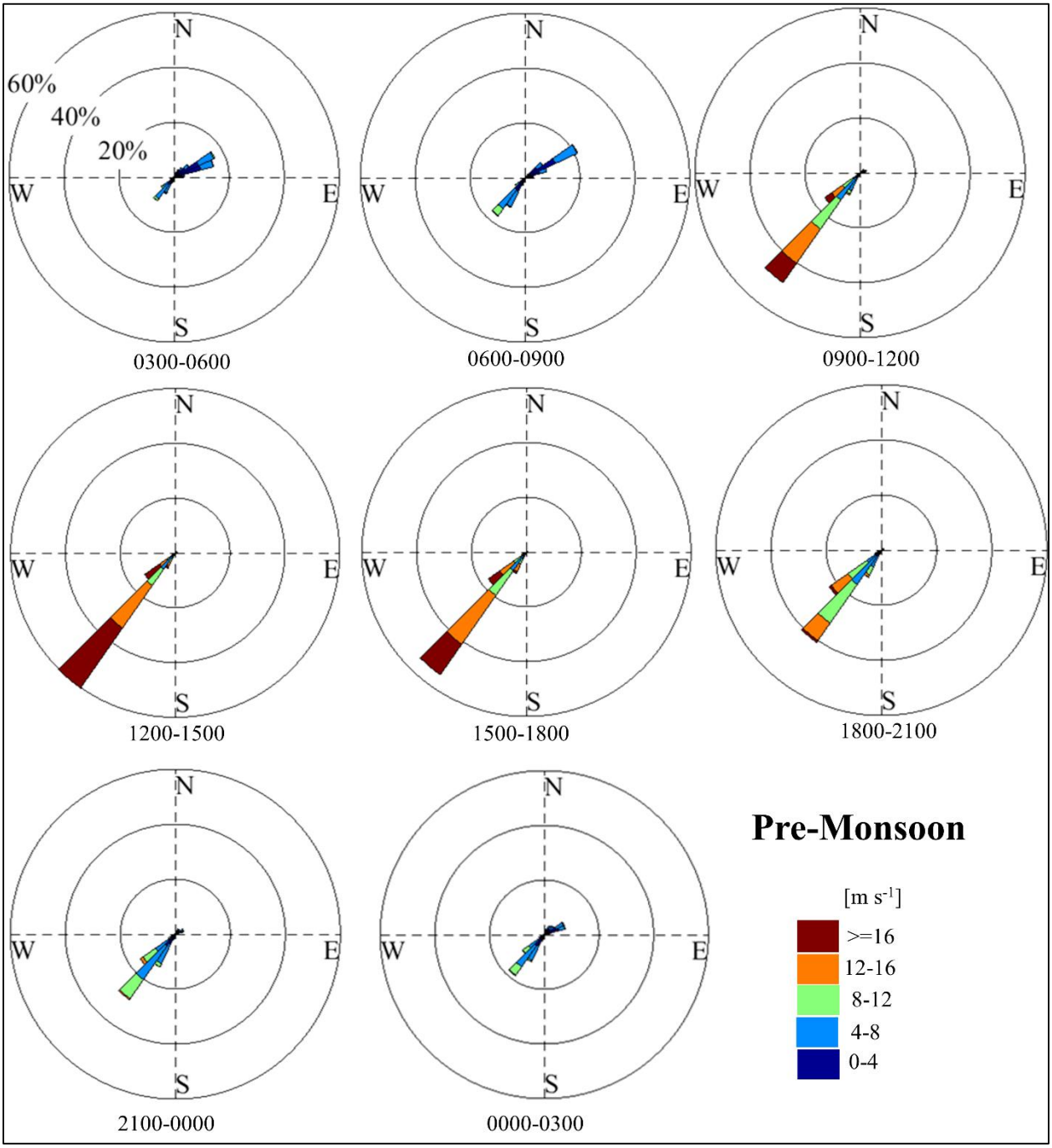

Figure 3a. Wind rose for pre-monsoon season – binned into 3-hour increments depiciting diurnal evolution in wind speed and direction at JSM_2.

5

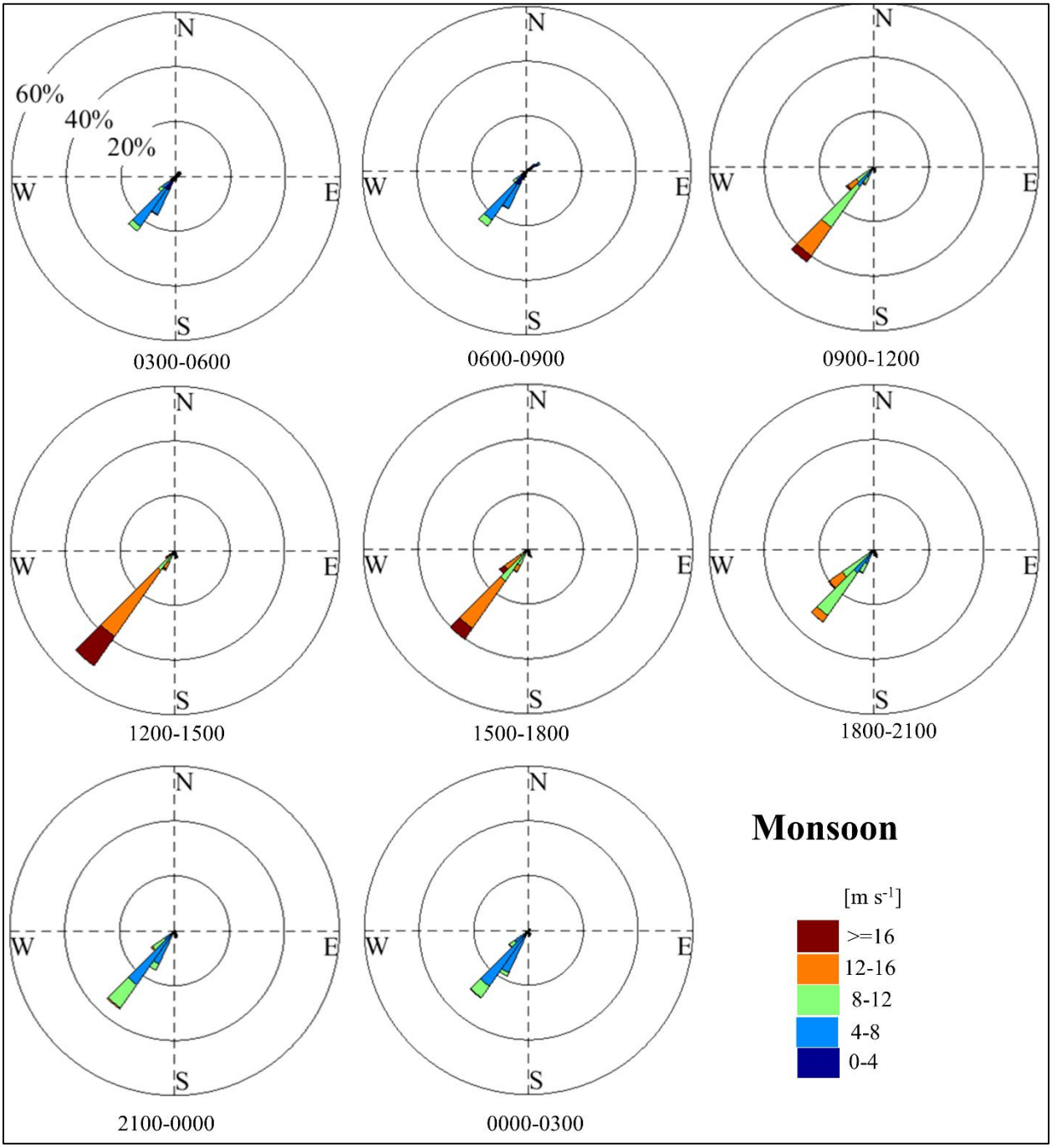

Figure 3b. Wind rose for monsoon season – binned into 3-hour increments depiciting diurnal evolution in wind speed and direction at JSM_2.

5

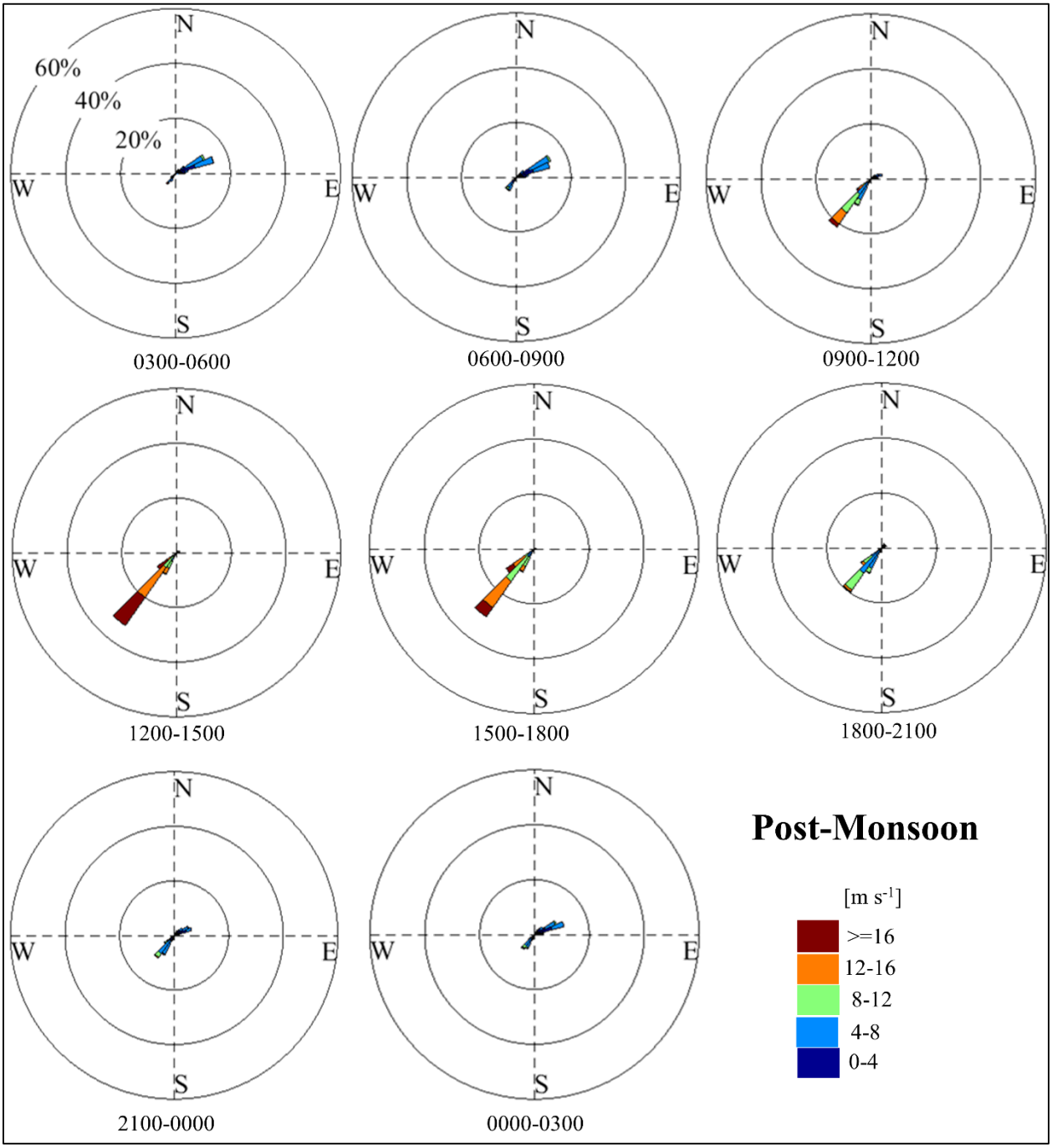

Figure 3c. Wind rose for monsoon season – binned into 3-hour increments depiciting diurnal evolution in wind speed and direction at JSM_2.

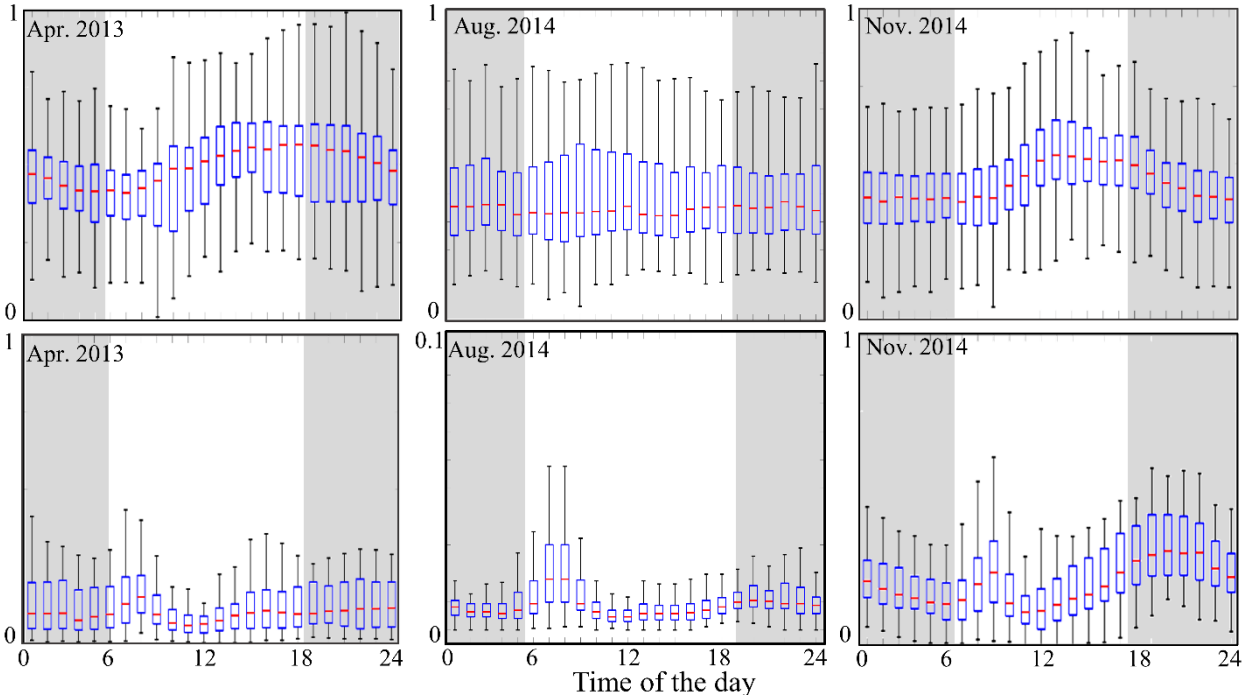

Figure 4. Box and whisker plots depicting the 90th, 75th, 50th, 25th, and 10th percentiles for normalized diel variability in O_3 (upper panels) and BC (lower panels) at JSM_STA during April 2013 (pre-monsoon), August 2014 (monsoon), and November 2014 (post-monsoon). Scale for August 2014 is from 0 to 0.1.

5

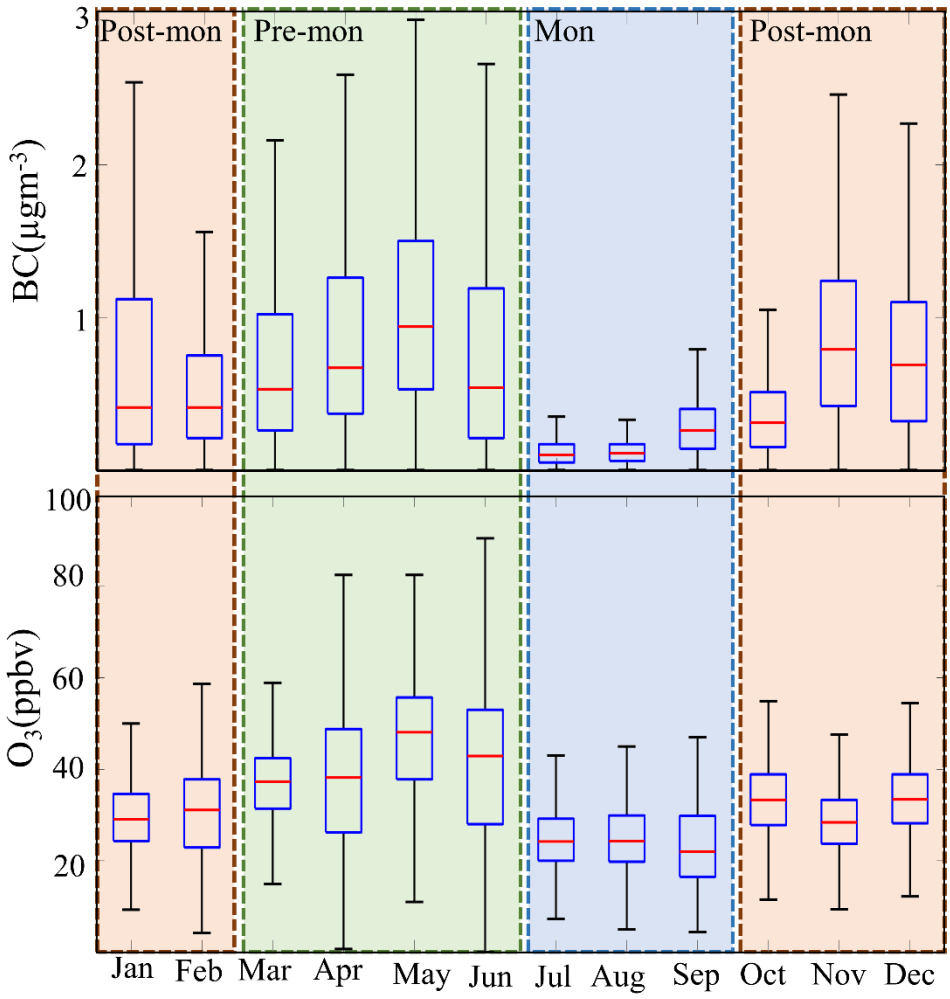

Figure 5. Box and whisker plots depicting the 90th, 75th, 50th, 25th, and 10th percentiles for monthly concentrations of BC (upper panel) and O_3 (lower panel) between January 2013 and August 2015 at JSM_STA. Orange shaded areas indicate the post-monsoon season (Post-mon), green shaded area indicates the pre-monsoon (Pre-mon) and blue are indicates the monsoon (Mon) season.

Table 2. Comparison of BC and O_3 concentrations (mean ±standard deviation) between high elevation Himalayan site NCO-P CNR and JSM_1.

Sites	Altitude (m)	Co-ordinates	Season	BC (μg m^{-3})	O_3 (ppb)
NCO-P CNR (Bonasoni et al., 2010)	5079	27.95° N, 86.81° E	Pre-monsoon	0.317 (±0.34)	60.9 (±8.4)
			Monsoon	0.049 (±0.06)	38.9 (±9.6)
			Post-monsoon	0.135 (±0.08)	46.3 (±5.0)
JSM_1	2800	28.87° N, 83.73° E	Pre-monsoon	0.891 (±0.45)	39.5 (±8.23)
			Monsoon	0.207 (±0.24)	25.1 (±6.48)
			Post-monsoon	0.714 (±0.42)	31.4 (±4.5)

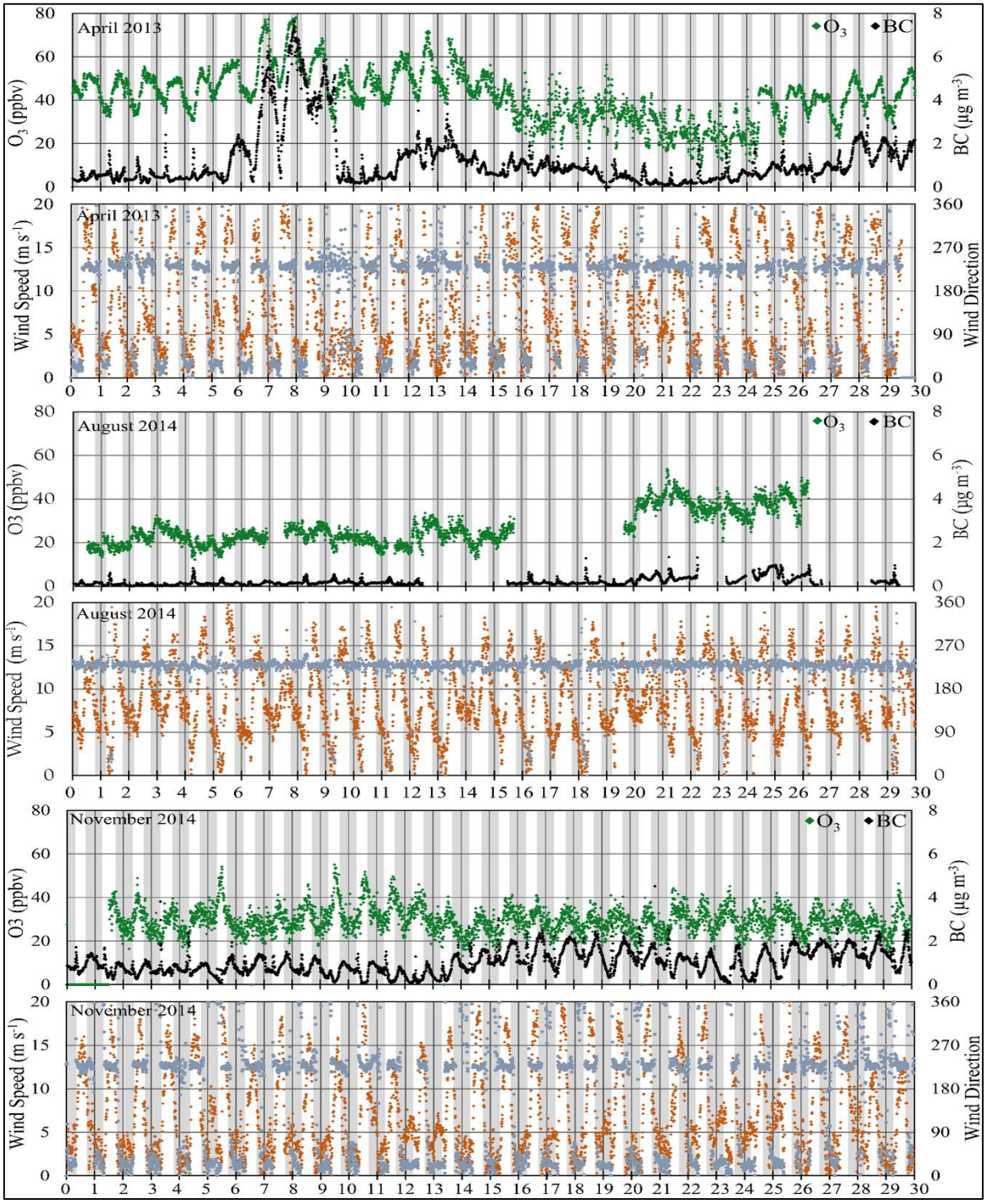

Figure 6. Variation in O_3, BC, and associated wind speed and direction at JSM_STA during (a) April 2013 (pre-monsoon), (b) July 2015 (monsoon), and (c) November 2014 (post monsoon). The grey shaded area denotes night.

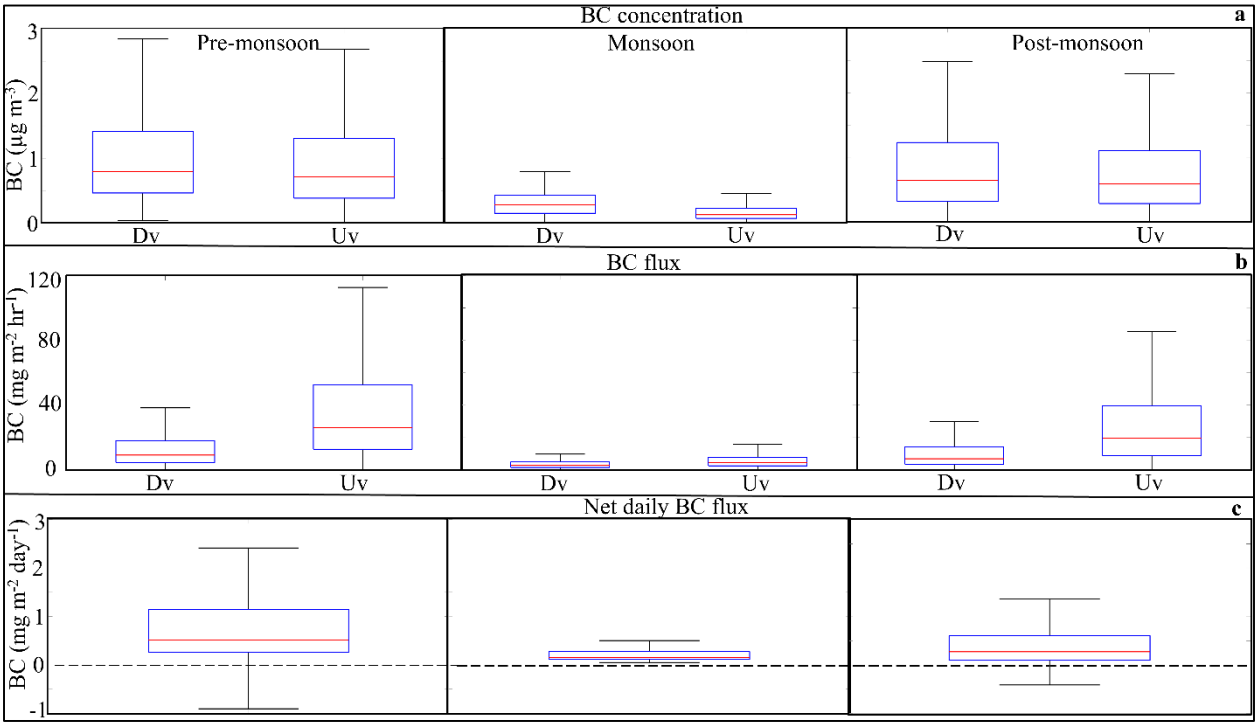

Figure 7. (a) BC concentration distribution with down-valley (Dv) and up-valley (Uv) flows in Jomsom, (b) calculated Dv and Uv flux for each season, (c) Net daily flux per season. The dotted line is panel c marks 0 mg m^{-2} day^{-1}. The red line represents 50th percentile, the edge of the box 25th and 75th percentile while the whiskers show maximum and minimum values.

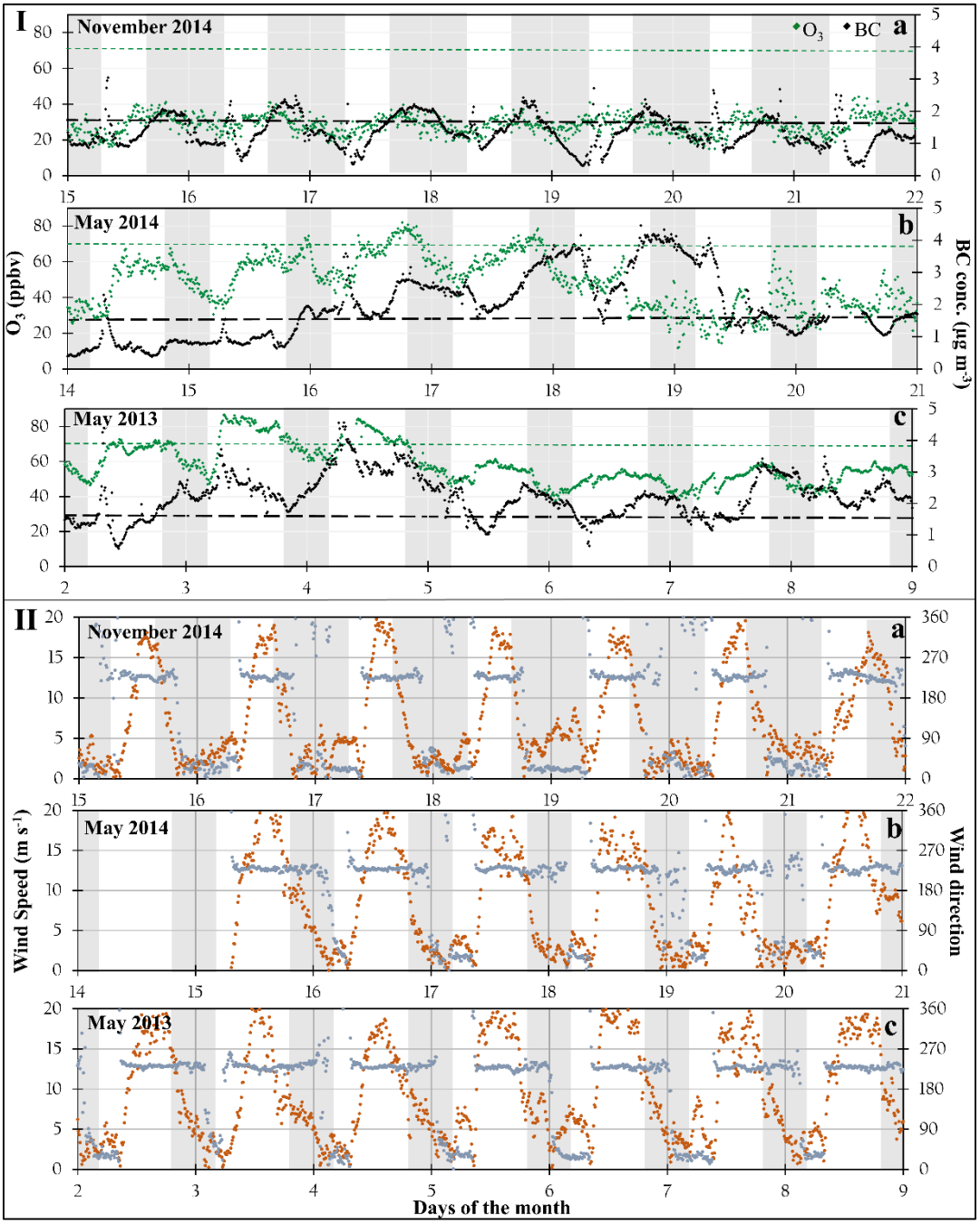

Figure 8. (I) Examples of extended periods with relatively high BC and O_3 concentrations at JSM_STA during November 2014 (Pattern A) and May 2014 (Pattern B) and May 2013 (Pattern C). The dashed black and greeen lines depict two-year averages for BC and O_3, respectively. (II) Corresponding wind direction and wind speed during the high BC and O_3 episodes. The orange dots represent wind speed, and the blue dots represent wind direction.

Table 3. List of enhanced BC episodes observed at JSM_STA and the concurring regional sources from MODIS (* Data is from January-July; $^{+}$ Incomplete O_3 data)

2013 (90th percentile : BC = 1.53 µg m^{-3} and O_3 = 49.5 ppbv)			
Month	**Episode Length**	**Episode type**	**Days with O_3 mixing ratio above 90th percentile**
Jan	6th – 15th	C	1
	28th – 31st	C	1^{+}
Feb	Jan 28th – Feb 2nd	C	1^{+}
Mar	1st – 3rd	A	0
	6th – 9th	A	0
	11th – 13th	B	0
	18th – 27th	B	4
Apr	6th – 10th	B	5
	12th – 14th	B	3
	27th – 30th	A	4
May	3rd – 11th	B	9
Oct	28th – 30th	A	No data
Nov	1st – 5th	A	No data
	23rd – 30th	A	0^{+}
Dec	17th – 24th	C	0^{+}
2014 (90th percentile: BC = 1.60 µg m^{-3} and O_3 = 56.8 ppbv)			
Month	**Episode Length**	**Episode type**	**Days with O_3 mixing ratio above 90th percentile**
Jan	13th – 15th	A	No data
Feb	Jan 31st – Feb 1st	A	No data
Mar	14th – 16th	A	No data
Apr	5th – 8th	B	2
	10th – 30th	C	15^{+}
May	Apr 10th – May 1st	C	15^{+}
	8th – 13th	B	6

	$17^{th} – 23^{rd}$	C	5^{+}
Jun	$5^{th} – 8^{th}$	B	3
	$10^{th} – 17^{th}$	B	8
Nov	$15^{th} – 30^{th}$	A	0
Dec	Nov 15^{th} – Dec 8^{th}	A	0
2015 (90^{th} percentile: BC = 1.47 µg m^{-3} and O_3 = 49.7 ppbv)			
Month	**Episode Length**	**Episode type**	**Days with O_3 mixing ratio above 90^{th} percentile**
Jan	$15^{th} – 17^{th}$	A	No data
	$21^{st} – 25^{th}$	A	No data
Feb	$21^{st} – 26^{th}$	A	No data
May	$6^{th} – 9^{th}$	A	0^{+}
	$18^{th} – 26^{th}$	A	8
	$29^{th} – 31^{st}$	B	3
Jun	$6^{th} – 12^{th}$	B	7